The Cryosphere Discuss., 5, 3323–3381, 2011
www.the-cryosphere-discuss.net/5/3323/2011/
doi:10.5194/tcd-5-3323-2011

The Cryosphere Discussions

Recent acceleration of ice loss in the Northern Patagonia Icefield based on an updated decennial evolution

P. López[1,2] and G. Casassa[1]

[1]Centro de Estudios Científicos (CECS), Arturo Prat 514, Valdivia, Chile
[2]Laboratoire Hydrosciences, UMR5569, CNRS – IRD, Universities 1 & 2, 34095 Montpellier Cedex 5, France

Received: 26 October 2011 – Accepted: 9 November 2011 – Published: 3 December 2011

Correspondence to: P. López (paulinalopez@cecs.cl)

Published by Copernicus Publications on behalf of the European Geosciences Union.

TCD
5, 3323–3381, 2011

Recent acceleration of ice loss in the Northern Patagonia Icefield

P. López and G. Casassa

Abstract

Ice elevation changes of the Northern Patagonia Icefield (NPI) were analyzed by comparing three Digital Elevation Models (DEM) corresponding to 1975 (constructed based on topographic maps), the SRTM DEM of 2000 yr and a SPOT 5 DEM of 2005. In addition, the glacier length fluctuations and the surface area evolution between 2001 and 2011 of 25 glaciers of the NPI were studied: the information extracted from the Landsat ETM+ satellite image of 11 March 2001 was compared to the measurements performed based on the Landsat ETM+ satellite image of 19 February 2011. From a global point of view, the majority of the studied glaciers thinned, retreated and lost surface between 2001 and 2011, only few glaciers (Leones, Nef, Pared Sur and Soler) located on the eastern side of the NPI have been stable. Glaciers located on the western side of the NPI suffered a stronger wasting compared to the glaciers located on the eastern side.

Overall, over the ablation areas of the NPI (below 1150 m a.s.l.) a more rapid thinning of 2.6 m yr^{-1} occurred between 2000 and 2005 yr compared to the period 1975–2000, in which a mean thinning of 1.7 m yr^{-1} was measured for the same zones of the NPI. For the whole period (1975–2005) the most important thinning of the ablation areas has been estimated for HPN-1 Glacier (4.4 m yr^{-1}) followed by Benito (3.4 m yr^{-1}), Fraenkel (2.4 m yr^{-1}), Gualas (2.1 m yr^{-1}) and Acodado glaciers, all of them located on the western side of the NPI.

Between 2001 and 2011, a noteworthy retreat of 1.9 km was experienced by Gualas Glacier and by Reichert Glacier with 1.6 km, both located on the north-western side of the NPI. On the south-western side of the NPI, during the same decennia, Steffen Glacier experienced a remarkable retreat of 1.6 km as well. During the 2001–2011 period, Steffen Glacier more than doubled its rate of retreat (compared to the 1979–2001 period) and experienced the disintegration of its main front as well as a lateral tongue that retreated 3.1 km. The most significant retreat observed on the eastern side was experienced by Colonia Glacier (1 km).

TCD

5, 3323–3381, 2011

Recent acceleration of ice loss in the Northern Patagonia Icefield

P. López and G. Casassa

Area loss was also relevant during the period 2001–2011. Overall, the icefield experienced a reduction of 50.6 km^2 which represents a 1.3 % relative to the surface area calculated for 2001 yr. The most remarkable surface reduction was observed for HPN-1 Glacier that lost 3.2 % of its surface estimated in 2001, followed by Steffen Glacier (2.8 %).

We suggest that the glacier shrinking observed in the NPI is controlled firstly by atmospheric warming, as it has been reported in this area. Nevertheless, updated climatic studies are needed in order to confirm this suggestion. If the detected past climate trends persist, in the future, glaciers of the NPI will continuous or even increase their rate of shrinking generating important consequences for this region like the production of Glacier Lake Outburst Flood events or the decrease of the melt-water runoff in the long-term future.

1 Introduction

The reported past and ongoing climatic changes have been dramatically affecting the glacierized areas of the world (IPCC, 2007). Indeed, glaciers located on the Andes Cordillera have also shown a clear reduction during the preceding decades.

Located in the Austral region (between 46° S–51°30′ S and 72° W–73° W) and accounting for more than 60 % of the glacierized surface area of South America (Aniya, 2007), the Northern Patagonia Icefield (NPI) and the Southern Patagonia Icefield (SPI) cover 13 000 km^2 (Aniya, 2001; Aniya et al., 1997) and 4197 km^2 (Rivera et al., 2007), respectively.

The Patagonian Icefields are a unique natural laboratory (Casassa et al., 2002). They cover such a large area (>17 000 km^2) which has a very rich biodiversity. Moreover, they represent a large potential for water resources.

Due to their temperate nature, the icefields are very sensitive to climate change – both local and worldwide – since any surplus of energy will induce ice melting (Hock, 2005; Oerlemans, 2001). Therefore, the understanding of their current nature is a key

TCD
5, 3323–3381, 2011

feature to make predictions of their future evolution (Casassa et al., 2002). At present, the current understanding of the relation between Patagonian glaciers and climate is limited and accurate studies are needed.

Glaciers composing the NPI and the SPI have experienced an accelerated and enhanced wasting during the preceding decades (Aniya et al., 1997, 2000; Casassa, 1995; Casassa et al., 1997; Glasser et al., 2011; López et al., 2010b; Skvarca and De Angelis, 2002). The main consequences of the enhanced wasting of the Patagonian glaciers include: (i) the contribution of meltwater to sea level rise (Rignot et al., 2003) ; (ii) the increase of Glacier Outburst Flood (GLOF) events (Casassa et al., 2010) and (iii) the decrease of the water runoff in the long-term future (Casassa et al., 2009; López et al., 2010a; López et al., 2011).

The majority of the glaciological investigations performed for the NPI have concentrated in reporting surface and frontal changes. Only few investigations studied ice elevation changes, mainly due to the difficulties in carrying out field measurements and the lack of remote sensing data allowing the construction of Digital Elevation Models (DEM).

The aim of this investigation is to estimate ice elevation changes of NPI glaciers between 1975, 2000 and 2005 and to analyze the spatial distribution of the ice elevation changes inside the icefield. In addition, glacier length and surface changes are updated for the period 2001–2011.

2 The Northern Patagonia Icefield

The NPI (Fig. 1) is located between 46°30′ S and 47°30′ S along 73°30′ W. It covers a total area of 4197 km^2 (including rock outcrops) (Rivera et al., 2007) and extends for nearly 125 km north-south between Grosse and Steffen glaciers, with a maximum width of 71 km in a west-east direction between the frontal tongues of San Quintín and Soler glaciers. The highest elevation is the summit of Mount San Valentín 4032 ± 1 m above sea level (a.s.l.) located in the northeastern area of the NPI, and the minimum altitude is at sea level on the tidewater Laguna San Rafael located on the western side of the NPI at the calving front of San Rafael Glacier.

Because of the west-east precipitation gradient and topography, with the highest summits located closer to the eastern margin of the NPI, the glaciers are larger on the western side than on the eastern side.

Using a Landsat ETM+ satellite image of 11 March of 2001, Rivera et al. (2007) estimated a mean ELA for the NPI of 1150 m a.s.l. According to previous studies, the ELA presents strong spatial variations inside the icefield, being 500 m lower on the western side than on the eastern side (Ohata et al., 1985). Barcaza et al. (2009) stated that the average ELAs range between 870 m and 1529 (±29 m), with lower altitudes on the west side. Most NPI glaciers have calving fronts in freshwater lakes. Only one glacier, San Rafael, has a tidewater calving front (Warren et al., 1995).

The NPI was explored for scientific purposes for the first time by Dr. F. Reichert in 1921 (Casassa and Marangunic, 1987). Since then, many scientific expeditions have taken place. The snout positions of the glaciers for the entire icefield were first described by Louis Lliboutry (1956) who used topographic maps at a scale of 1:250 000 and Trimetrogon aerial photographs (oblique and vertical) acquired in 1944/45. Starting in the 1960s, important scientific studies have been performed in Patagonia by Japanese glaciologists (Casassa and Marangunic, 1987), which have continued to the present day (Aniya, 2007).

The installation of a glaciological monitoring network allowing the regular survey on the field has been hampered by the big size of the NPI and the adverse weather conditions of the area. Prevailing cloud cover hampers as well the regular acquisition of optical satellite images. In spite of these limits, several investigations have been performed on the NPI which allow to characterize a generalized retreat and shrinkage during the last 60 yr (Aniya, 1992, 1999, 2001, 2007; Aniya et al., 1988, 2011; Aniya and Enomoto, 1986; Aniya and Wakao, 1997; López et al., 2010b; Rivera et al., 2007). According to Aniya (2007), variations in the length of 21 outlet glaciers in the NPI over the last 60 yr indicate that overall, glaciers retreated. Even though there have been significant variations in the glacier fronts, the retreat became more pronounced after the 1990s, with larger rates of retreat observed on the western side than on the eastern side. All of the above cited studies concluded that the primary cause of the retreat of Patagonian glaciers is the warming reported for this region (Carrasco et al., 2002; Ibarzabal et al., 1996; Rasmussen et al., 2007; Rosenblüth et al., 1995).

The reporting of ice volumetric changes of NPI's glaciers has been limited to a few studies. Using Digital Elevation Models (DEMs) and historical maps, ice elevation changes have been estimated for SPI and NPI between 1975 and 2000 by Rignot et al. (2003), who obtained a mean ice thinning of 0.76 $\mathrm{m\,yr^{-1}} \pm 0.1$ over an area of 3481 $\mathrm{km^2}$ for NPI and a mean ice thinning of 0.88 $\mathrm{m\,yr^{-1}} \pm 0.06$ over an area of 8167 $\mathrm{km^2}$ of SPI. For the NPI Rivera et al. (2007) estimated a mean thinning of $1.8 \pm 0.97\,\mathrm{m\,yr^{-1}}$ between 1975 and 2001. Both the studies of Rignot et al. (2003) and Rivera et al. (2007) cover mainly the ablation areas of the icefields, since the IGM (Instututo Geográfico Militar, Chile) DEM of 1975 and the ASTER DEM of 2001 have limited coverage of the accumulation area due to lack of stereoscopic vision over the flat snow-covered icefield.

3 Data

3.1 Digital elevation models

As mentioned before, the ice elevation changes were estimated by comparing three different DEMs of 1975, 2000 and 2005. Figure 2 and Table 1 show the surface covered by every DEM over the NPI.

According to Rivera et al. (2007) the ice area of the NPI calculated based on a Landsat satellite image of 11 March 2001 was 3953 $\mathrm{km^2}$. In Table 2, the percentage covered by the pair-wise comparison related to the total maximum extent of the NPI is shown in Table 2.

3.1.1 DEM of 1975

The DEM of 1975 used in this investigation was elaborated by Rivera et al. (2007) based upon contour lines of the 50 000 scale IGM regular cartography of 1975. The DEM has a spatial resolution of 50 m and a total vertical random error of 19 m (Rivera et al., 2007). According to Table 1 this DEM covers 1930 km^2 (48.8 %) of the whole NPI.

3.1.2 Shuttle Radar Topography Mission (SRTM) Digital Elevation Model (DEM)

The SRTM consisted of a specially modified radar system that flew onboard the space shuttle Endeavour during an 11-day mission in February 2000. The SRTM elevation data are available between latitudes of 60° N and 57° S.

The horizontal resolution of the SRTM DEM is 90 × 90 m and the absolute vertical accuracy is better than 9 m (Farr et al., 2007). According to the biases from the penetration of radar signals into snow and ice are negligible (Rignot et al., 2001).

According to Table 1 this DEM cover 3794 km^2 (95 %) of the whole NPI.

3.1.3 Spot5 stereoscopic survey of Polar Ice: Reference Images and Topographies (SPIRIT) products

The SPIRIT products include two DEMs (including a confidence mask) and one orthoimage. The SPIRIT products have been delivered in the framework of a program launched by SPOT Image with the purpose of support scientific researches focused on polar regions.

The DEMs have been acquired through the HRS (High Resolution Sensor) sensor onboard SPOT 5 (Système Probatoire de l'Observation de la Terre) satellite. The HRS sensor acquires pair of images in a single pass of the satellite. The HRS sensor acquires the DEMs in the panchromatic mode (0.48–0.71 µ) delivering stereoscopic pairs of 600 km by 120 km from which the DEMs are computed using different sets of

TCD
5, 3323–3381, 2011

correlation parameters according to the relief (Korona et al., 2009). The DEMs have a vertical accuracy of 10 m over ice free landscapes (90 % of confidence on surface slopes less than 20 %) and 40 m of spatial resolution.

The ortho-images provided on the SPIRIT product have an absolute horizontal precision of 30 m and 5 m of spatial resolution (Korona et al., 2009). In this investigation a SPIRIT product including a DEM (version 2) acquired over NPI on 13 May 2005 along with the corresponding reliability masks and an ortho-image have been used.

According to Table 1 this DEM cover 2946 km^2 (74.5 %) of the whole NPI.

3.1.4 ICESat data

ICESat satellite was lauched on 12 January 2003. The Geosciences Laser System (GLAS) onboard ICESat operates with Infrared and Visible laser light pulses at 532 nm. GLAS produces 16 data products including levels 1A, 1B and 2 (processing levels). Data products, distributed by the NSIDC National Snow and Ice Data Center (NSIDC), include surface elevation acquired with a 33 days repeat cycle, in a near circular and near polar orbit slightly inclined relative to the Equator covering between 86° N and 86° S. The orbital altitude is 600 km. Laser footprints have a diameter of ~70 m separated by 170 m, a vertical accuracy of 7 m and data is geolocated with Jason Topex Poseidon Ellipsoid (slightly different than WGS 84 and EGM 96) (Zwally et al., 2002).

Ice elevation changes over the NPI cannot be analyzed using exclusively ICESat data since along tracks and crossover points cover a small portion of the NPI (Fig. 3). Nevertheless, the available ICESat data over the non glacierized area was used in this study as ground truth considering its higher vertical accuracy compared to the other DEMs taken into consideration.

3.2 Satellite imagery

3.2.1 Landsat images

The Landsat (Land Satellite) series of satellites has been providing visible and near-infra red imagery of the Earth's surface (up to a latitudinal limit of $\sim \pm 82.5°$) since 1972 (Bamber and Payne, 2004). There are three types of Landsat images: Landsat MSS (Multispectral Scanner), Landsat TM (Thematic Mapper) and Landsat ETM+ (Enhanced Thematic Mapper Plus). Landsat MSS and Landsat ETM+ were used in the present study (Table 3) with the purpose to calculate glacier length and surface changes of the NPI. The satellite images available allow to study a surface of 3530 km^2 corresponding to 25 glaciers of the NPI, the remaining area was not included in this investigation due to problems of identification (i.e. cloud cover).

Landsat MSS images have a spatial resolution of 57×79 m and five spectral bands (two visible bands, two near infrared bands and one thermal band). The ETM+ images (spatial resolution 28.5 m) include seven spectral bands (three visible bands, one near infrared band, two short infrared bands and one thermal band).

4 Methods

From a general point of view, every satellite image and DEM used in this investigation was projected to the UTM cartographic projection (Zone 18) and to the WGS 84 geodetic datum. Further on, different methods, described in this section, have been applied for the surface, glacier length and ice elevation changes estimations.

4.1 Surface and glacier length changes

The ice divides estimated by Rivera et al. (2007) have been taking into account for the surface and glacier length change estimation. The comparison has been done

TCD
5, 3323–3381, 2011

using the ETM+ Landsat satellite images of 2001 and 2011 (Table 3), thus updating the analysis of Rivera et al. (2007).

The lengths of glaciers of the NPI calculated by López et al. (2010b) have been updated for 2011 and, additionally, new glaciers have been included in the database. The same criteria considered by López et al. (2010b) have been applied in this investigation: (i) glacier length is represented by a line which corresponds to the longest distance followed by the glacier; (ii) the length was measured from the lowest to the highest point of the glacier; (iii) the origin is the central position of the glacier's front; (iv) the length/distance follows the central position of the glacier tongue and; (v) the length follows surface flow trajectories if they are identifiable on the satellite image. Criteria (i), (ii) and (iii) were respected for every glacier, while the application of criteria (iv) and (v) depended on the glacier's shape and surface characteristics.

4.2 Ice elevation changes

Two main steps were followed before comparing the DEMs over the glacierized areas: (i) the horizontal shift and coregistration; and (ii) the estimation of the bias with the elevation.

4.2.1 The horizontal shift and coregistration

When two DEMs have been produced with the same cartographic projection and geodetic parameters, it is expected that no matching errors may exist. However, several investigations showed that an horizontal shift could exist when DEMs are compared (Berthier et al., 2006, 2007; Nuth and Kääb, 2011). Those differences may appear since every DEM has errors that depend on the sensor and the method applied to construct the model. For instance, Kääb (2005) described the errors associated to DEMs derived from optical satellite stereo.

Two DEMs of the same terrain surface that are not perfectly aligned experience a characteristic relationship between elevation differences and the direction of the terrain

TCD
5, 3323–3381, 2011

(aspect) that is precisely related to the x-y-shift vector between them (Nuth and Kääb, 2011). Based on this relationship Nuth and Kääb (2011) proposed the universal coregistration method in order to reduce the horizontal shift appeared when two DEMs are compared.

The universal coregistration method is based on a simple relation between the difference of elevation and the slope and aspect of the terrain (Nuth and Kääb, 2011). The magnitude and the direction of the shift are calculated on the non glacierized area since there no change on elevation must be expected over time.

The shift is calculated through the following relation:

$$dh/\tan(\alpha) = \boldsymbol{a} \times \cos(\boldsymbol{b} - \psi) + c \quad (1)$$

$$c = dh/\tan(\alpha)$$

Where: *dh*: difference of elevation; α: the terrain slope; ***a***: the magnitude of the shift; ***b***: the direction of the shift; ψ: the aspect of the terrain.

Once ***a*** and ***b*** values are calculated (trough Eq. 1), *DX* and *DY* are estimated by a trigonometric relation considering the magnitude of the shift vector ***a*** and the direction of the shift vector ***b*** (Fig. 4). The DEM is shifted according to the values obtained for *DX* and *DY*, this process is iterative until ***a*** is less than 0.5 or/and the standard deviation is less than 2 % (Nuth and Kääb, 2011).

4.2.2 The bias with elevation

A bias with elevation has been identified in several studies of ice elevation changes (Berthier et al., 2006, 2007; Berthier and Toutin, 2008; Nuth and Kääb, 2011). According to Nuth and Kääb (2011) an elevation dependent bias can for instance result from an uneven spatial distribution of the GCPs in the x-y-z-planes which leads to a poorly resolved stereo orientation that could cause a distortion of the z-scale in the measurement of parallaxes. Berthier et al. (2006) detected an altitudinal biases of SRTM data for the high mountain areas of the French Alps, however, Paul (2008) suggested that this bias could be related to the spatial resolution of the compared DEMs.

TCD
5, 3323–3381, 2011

To estimate this bias when two models are compared pair-wise, the difference of elevation over the non glacierized area is plotted as function of the elevation and subsequently a polynomial function is fixed. If any bias with elevation exists, *dh* is then corrected for every interval of elevation using the polynomial equation (Berthier et al., 2006).

5 Results

5.1 Ice elevation changes

The ice elevation changes were calculated by comparing DEMs of 1975 (from topographic maps), 2000 (SRTM) and 2005 (SPOT 5). Every DEM was resampled to 60 m of spatial resolution (pixel size) since it represents a mean spatial resolution between the footprints of the ICESat data, SPOT 5 DEMs and the DEM 1975.

The horizontal shift and coregistration of every DEM was done related to ICESat data. The horizontal shift is estimated for the non glacierized area by computing first, the difference of elevation (hereafter *dh*). For that purpose a mask was designed excluding the ice and snow covered area as well as rivers and lakes. The mask must be as precise as possible since if the *dh* is calculated in areas where changes could be observed over time, a bias will be introduced on the coregistration process. In addition, for the SPOT DEMs the confidence mask delivered with SPIRIT products (Korona et al., 2009), was considered as well to exclude all values with less than 50 % of confidence. Then, *dh* is calculated by subtracting every DEM to ICESat data. Further on, the slope and terrain aspect were computed.

In order to verify if any bias exists for *dh* related to the slope and aspect (horizontal shift and coregistration error as described before), $dh/\tan(\alpha)$ was computed for every pixel. The values obtained were plotted related to the terrain aspect as shown in Fig. 5. For every DEM a bias of *dh* has been detected since their $dh/\tan(\alpha)$/aspect curve has a sinusoidal shape (Nuth and Kääb, 2011) (Fig. 4). A sinusoidal shape has also been identified by Rivera et al. (2007) comparing the DEM 1975 and a DEM derived from ASTER satellite images of 2001 and 2002 yr.

Therefore, for every model the horizontal shift was estimated and then coregistered. In order to calculate the horizontal shift, first $\mathbf{a}$ and $\mathbf{b}$ were calculated according to Eq. (1). Then, the shift in East/West direction (DX) and in the North/South direction (DY) was estimated and the DEMs coregistered accordingly (Table 4).

The shifted process was done in an iterative way until the criteria for $\mathbf{a}$ (Sect. 4.2.1) was respected. The original and shifted values of every DEM are shown in Fig. 6.

Once every model was coregistered to ICESat, they were compared pairwise: 1975–2000, 2000–2005 and 1975–2005 over the non glacierized area (Table 5). Before estimating the ice elevation changes, the bias of dh with elevation was verified. With that purpose the terrain was divided into elevation bands of 100 m and the mean dh was computed for every interval of elevation. Then, a scatter plot was constructed for dh as function of the elevation and a curve was fitted using a polynomial equation. The polynomial equation was used to correct the dh for the 1975–2000 and 1975–2005 pair of DEMs for which a bias of 0.6 m/100 m and 0.7 m/100 m was calculated, respectively.

Ice elevation changes were computed for 1975–2000, 2000–2005 and 1975–2005 by subtracting every pair of DEMs. Mean thinning rates have been calculated for the entire icefield (including accumulation areas). According to Table 6, between 1975 and 2000 the NPI (over an area of 1850 km^2, Table 2) thinned at a rate of 0.73 $m\,yr^{-1}$ and between 2000 and 2005 a higher rate of 1.12 $m\,yr^{-1}$ was calculated for a surface of 2910 km^2 (Table 2).

Ice elevation changes have been also calculated for the ablation areas of the NPI glaciers. For that purpose, the overall ELA of 1150 m a.s.l. for the NPI estimated by Rivera et al. (2007) has been taken into account. As shown in Table 7, a mean thinning rate of 1.7 $m\,yr^{-1}$ was calculated for the period 1975–2000 below the mean ELA of 1150 m a.s.l. That rate of thinning was higher during the period 2000–2005, resulting in a thinning rate of 2.6 $m\,yr^{-1}$.

Elevation changes above the mean ELA were not delivered in this investigation since the data available cover merely the accumulation areas of the NPI. However, according to Table 2, the pair-wise comparison of DEMs of 2000 and 2005 cover 70 % of the total accumulation area of the NPI. For that pair-wise of DEMs, a small thinning of 0.08 m was estimated over the mean ELA of 1150 m a.s.l.

Rignot et al. (2003), calculated the contribution of the Patagonian glaciers to the sea level rise by comparing the DEMs from the IGM topographic maps of 1975 and the SRTM DEM of 2000. In addition, Rivera et al. (2007) estimated ice elevation changes over the ablation areas of some glaciers of the NPI by comparing the DEM of 1975 and the ASTER DEM of 2000.

In this paper, ice elevation changes between 1975 and 2000 were also calculated and compared to those obtained in previous studies. As shown in Table 8 no significant differences exist between the results obtained by Rignot et al. (2003), Rivera et al. (2007) and the results obtained in this study. This comparison allows validating our results.

5.1.1 Variations 1975–2005 (per glacier)

The surface of the NPI covered by the DEMs used in this investigation are shown in Table 1. In addition, the surface covered by the pair-wise of DEMs (for the whole NPI, the accumulation ad ablation area) is showed in Table 2 along with the corresponding percentage of the maximum extent of the whole icefield, the accumulation and ablation areas.

The mean thinning rates of the ablation areas (below the ELA estimated by Rivera et al. (2007) of glaciers of the NPI for the period 1975–2005 are shown in Fig. 7. As it is possible to observe, 13 glaciers thinned between 0 and 1 m yr^{-1}, 6 between 1 and 2 m yr^{-1} and 5 between 2 and 4 m yr^{-1}.

The highest thinning was observed for HPN-1 (4.4 m yr^{-1}) followed by Benito (3.4 m yr^{-1}), Fraenkel (2.4 m yr^{-1}), Acodado (2.1 m yr^{-1}), Strindberg (1.7 m yr^{-1}) and

San Quintín (1.6 m yr^{-1}) glaciers. All of the listed glaciers are located on the western flank of the NPI.

The lowest thinning was observed for Pared Sur Glacier (1.2 m yr^{-1}) located on the south-eastern side of the NPI. The most important thinning for the glaciers located on the eastern side of the NPI are observed for Soler and Cachet glaciers, both with a thinning of 2.2 m yr^{-1}.

5.1.2 Variations 1975–2005 (as a function of elevation)

The mean ice elevation changes between 1975 and 2005 of the NPI as a function of elevation (between 100 m and 2500 m) are shown in Fig. 8. In the upper areas of the NPI, (between ~1300 and 2500 m) the ice elevation changes are positive, indicating a thickening of about 20 m which does not increase with elevation. According to Rivera et al. (2007), the thinning for the period 1975–2001 appears below 1200 m a.s.l. In accordance with Fig. 8, for the period 1975–2005, thinning is observed below 1300 m a.s.l. indicating and a small thickening is seen above 1300 m a.s.l.

5.2 Glacier length changes

Glacier lengths fluctuations between 2001 and 2011 have been calculated for 25 major NPI glaciers (Table 9). A general glacier retreat has been observed for the whole NPI. As shown in Figs. 9 and 10, the strongest retreat has been observed for Gualas Glacier (1.9 km), Steffen Glacier (1.6 km) and Reichert Glacier (1.6 km). The smallest retreat has been observed for San Quintín, San Rafael and Nef glaciers with –0.01 km each.

The interpretation of Fig. 9 allows analysing the glacier retreat according to the glacier location. As shown in Fig. 9, on the northern area of the NPI a significant retreat is observed for Reichert (1.6 km) and Gualas (1.9 km) glaciers. On the south-western area, Fraenkel (0.5 km), Strindberg (0.7 km), HPN-1 (0.9 km), Acodado (1 km) and Steffen (1.6 km) glaciers retreated significantly as well. On the eastern side of the NPI the highest retreat is observed for Colonia Glacier (1 km) followed by Fiero

TCD
5, 3323–3381, 2011

(0.5 km), Pissis (0.5 km) and Pared Norte (0.4 km) glaciers. The rest of the glaciers located on the eastern side retreated up to 0.3 km.

The rates of glacier retreat of the studied glaciers have been compared between the periods 1979–2001 and 2001–2011. As shown in Fig. 11, a significant increase of the rate of retreat is observed between both periods for Gualas (0.27 km yr^{-1}), Steffen (0.09 km yr^{-1}), HPN-1 (0.08 km yr^{-1}), Colonia (0.07 km yr^{-1}) and Acodado (0.05 km yr^{-1}) glaciers.

A different situation is observed for San Rafael, San Quintín, and Nef glaciers. Those glaciers experienced the major retreats of the NPI between 1979 and 2001, however, during the period 2001–2011 their rate of retreat decreased significantly of 0.17 km yr^{-1}, 0.09 km yr^{-1} and 0.15 km yr^{-1}, respectively.

Several glaciers like Fiero, Leones, Soler, Arco, Pared Sur, Pared Norte, Pissis, U-4 and HPN-4 maintained a small rate of retreat (between 0.01 and 0.07 km yr^{-1}) during both periods (Fig. 11).

5.3 Area changes

Area changes between 2001 and 2011 have been estimated for the 25 studied glaciers of the NPI (Table 10). A total decrease of 50.6 km^2 (1.3 % of reduction compared to the surface area of 2001) of glacierized surface has been calculated (Fig. 12). The most significant shrinkage is observed for San Quintin Glacier (13.2 km^2), Steffen Glacier (12 km^2), HPN-1 Glacier (4.9 km^2) and Acodado Glacier (4.8 km^2). An opposite situation was observed for Soler, Leones, Nef and Pared Sur glaciers which lost not more than 0.2 km^2 during the same period (Figs. 12 and 13).

Given the size differences among the glaciers of the NPI, the surface changes must be therefore interpreted in terms of their original area in 2001, as shown in Fig. 14. The largest shrinkage has been experienced by HPN-1 Glacier with a loss of 3.2 %, followed by Steffen Glacier (2.8 %). Gualas, Reichert and Fraenkel glaciers lost 2.4 % and Strindberg Glacier 2 %. All the mentioned glaciers are located on the western side of the NPI, which is illustrated in Fig. 12.

On the eastern side of the NPI, the highest shrinkage was observed for Pissis (1.9 %), followed by Cristal (1.5 %) and Colonia (1.1 %) glaciers. The rest of the glaciers located on the eastern side of the NPI experienced a surface reduction of not more than 1 % in the 10-yr period. In Fig. 14, the percentage of surface reduction of the period 1979–2001 is compared to that calculated for the period 2001–2011. The most striking feature is the enhanced shrinkage experienced by Steffen Glacier which lost 2.8 % of its surface during 2001–2011. Between 1979 and 2001, Steffen Glacier shrunk 2.6 % at a rate of 0.5 $km^2 yr^{-1}$, therefore, in 2001–2011 this glacier more than doubled its rate of shrinking. Gualas Glacier increased its rate of shrinking as well from 0.14 % in 1979–2001 to 0.28 % in 2001–2011.

The rate of shrinkage of San Rafael Glacier decreased from 0.7 $km^2 yr^{-1}$ between 1979 and 2001 to 0.3 $km^2 yr^{-1}$ during the period 2001–2011. A similar situation is observed for San Quintín, Soler and Pared Sur, since those glaciers reduced their shrinking rate by 0.2 $km^2 yr^{-1}$, 0.1 $km^2 yr^{-1}$, 0.4 $km^2 yr^{-1}$ and 0.1 $km^2 yr^{-1}$, respectively.

Between both periods, a few glaciers maintained their rate of shrinkage, such as Reichert (0.2 $km^2 yr^{-1}$), Acodado (0.5 $km^2 yr^{-1}$), and Benito (0.3 $km^2 yr^{-1}$).

6 Discussion

As a result of the analysis of the ice elevation changes, glacier length and surface area fluctuations of 25 glaciers of the NPI, it is observed that all the studied glaciers have been thinning, retreating and losing surface during the decennium 2001–2011. The glaciers located on the north-western (Gualas and Reichert) and on the south-western (HPN-1, Acodado and Steffen) sides of the NPI experienced the largest ice loss. According to Barcaza et al. (2009), winter snow cover accumulation indicates higher elevations (relative to the glacier snout) of the transient snowlines in the west and thus, one of the reasons for the higher retreating rates observed on the west side is that the lower part of the ablation area is likely exposed to year-round ablation.

The shrinkage and retreat experienced by Steffen, Reichert and Gualas glaciers are especially noteworthy, for that reason those glaciers are analyse in more detail in the present section.

6.1 Steffen Glacier

Steffen Glacier is located at 47°32′ S and 73°42′ W (Fig. 15) draining the southern margin of the NPI. This freshwater calving glacier is the third largest glacier of the NPI after San Rafael and San Quintín Glaciers (Aniya, 1988). Steffen stretches between its highest altitude of 3365 m a.s.l. and its lowest altitude of 25 m a.s.l. The ELA of Steffen Glacier was first estimated at 900–1000 m by Aniya (1988). Later, Rivera et al. (2007) measured an ELA of 1074 m a.s.l. using Landsat satellite images of 10 February 2001.

In the framework of studies of the entire NPI, frontal, surface and volume fluctuations of Steffen Glacier have been reported earlier through the analysis of optical satellite images. Rivera et al. (2007) measured a surface area of 454 km^2 in 2001 and estimated an ice area loss of 12 km^2 equivalent to 2.6 % of the 1979 area (the largest of the southern margin of the NPI).

The front of Steffen Glacier has been retreating during the last 60 yr (Aniya, 1988, 1992, 1999, 2007; Aniya and Wakao, 1997; López et al., 2010b). According to López et al. (2010) the length of Steffen Glacier retreated 2.1 km between 1944–1945 and 2003. This reported glacier retreat was not gradual since in only 14 yr (between 1987 and 2001) the glacier retreated 1.4 km. According to Aniya et al. (1997) Steffen Glacier experienced a rapid calving retreat after 1986, which was further accelerated between 1991 and 1994, due to extensive calving in the proglacial lake of the southern front.

Between 2001 and 2011, Steffen Glacier experienced an impressive shrinkage acceleration, with a loss of 2.8 % of its 2001 area. This means that in only 10 yr (2001–2011) this glacier shrunk the same percentage than it did in the previous 22 yr (1979–2001), doubling its shrinking rate from 0.5 to 1.2 $km^2\,yr^{-1}$.

Between 2001 and 2011, Steffen Glacier experienced a total surface reduction of 12 km^2. This shrinking has mainly occurred on its ablation area since the three main

TCD
5, 3323–3381, 2011

Recent acceleration of ice loss in the Northern Patagonia Icefield

P. López and G. Casassa

tongues of Steffen Glacier have experienced strong reduction as seen in Figs. 15 and 16. The main tongue lost 3.9 km^2. The other two most important tongues of this glacier, located on its western side, namely F1 and F2 in Fig. 16, shrinked 4 km^2 and 1.8 km^2, respectively. Together the frontal loss of these 3 tongues accounted for 9.7 km^2, representing 81 % of the total ice loss of the glacier.

Between 2001 and 2011, the main front of Steffen Glacier retreated 1.6 km which is equivalent to the retreat registered in 1979–2001, therefore, the rate of retreat more than doubled between 2001 and 2011. Between 2001 and 2007, the glacier retreated 810 m and subsequently, between 2007 and 2011 it retreated another 790 m. As shown in Fig. 16, the satellite image of February 2011 shows the Steffen Lake covered by blocks of ice produced by the rapid retreat of the glacier's front.

As seen in Fig. 16, the front F1 did not experience a clear retreat between 2001 and 2007, however, on the image of April 2007 it is possible to observe that its corresponding tongue was very crevassed and extremely stretched. According to Fig. 16, between 2007 and 2011 the F1 tongue disintegrated, retreating 3.1 km and representing a retreat 13 times larger than the one recorded in 1979–2001.

The front F2 retreated 1.5 km between 2001 and 2011. As shown in Fig. 16, the tongue F2 was already disintegrated in April 2007. Therefore, between 2007 and 2011 no significant fluctuations have been produced at this front.

One of the main impacts of the accelerated retreat of Steffen Glacier is the clear increase of the surface area of its main proglacial lake (from 4.2 km^2 in 2001 to 9.4 km^2 in 2011), generating the increase of the river section of Rio Huemules. The described modifications on the drainage network of this catchment basin have alarmed the population living downstream of Rio Huemules (F. Espinoza, personal communication, 2011).

6.2 Gualas Glacier

Gualas Glacier is located on the north-western side of the NPI at 46°33′ S and 73°40′ W stretching between its highest elevation of 3910 m a.s.l. and 130 m a.s.l. (Aniya, 1988).

The ELA was estimated by Aniya (1988) between 750 and 900 m. Subsequently, (Rivera et al., 2007) estimated a rise of the ELA locating it at 1087 m.

Harrison and Winchester (1998) used dendrochronology to date historical fluctuations of Gualas Glacier. Harrison and Winchester (1998) identified vegetation trimlines dating to AD 1876, 1909 and 1954 showing that the wasting and retreat of Gualas Glacier mirrored the patterns found at San Rafael and San Quintín glaciers.

As the majority of the glaciers of the NPI, this temperate glacier experienced an accelerated shrinking since the beginning of the 20th century (Glasser et al., 2011). The fluctuations of Gualas Glacier have been reported in particular since 1944–1945, year for which the first glaciological map of the icefield has been available (Lliboutry, 1956).

By 1944–1945, Gualas Glacier had two different fronts draining to the north-western and south-western side of the NPI. The north front of Gualas Glacier experienced a retreat of 1.3 km between 1945 and 1979 and continuous retreating at a similar rate (20–30 m yr^{-1}) between 1985–1986 and 1990–1991 (Aniya, 1992).

Until 1991, Gualas Glacier calved into 2 proglacial lakes, however, by 1996 the glacier area separating both lakes retreated and subsequently a channel appeared (Aniya and Wakao, 1997).

After 1996, Gualas Glacier continuously retreated. Between 1999 and 2000 the glacier retreated 700 m losing 0.40 km^2 of surface area (Aniya, 2001) as a consequence of the previous stretching of its tongue. During the period 1945–2001, Gualas Glacier retreated 2.5 km (López et al., 2010b).

Gualas Glacier experienced a thinning of 50 m between 1975 and 2000 (Rivera et al., 2007). Our results show that the rate of thinning of Gualas Glacier between 2000 and 2005 increased by 0.7 m yr^{-1} compared to the rate registered for the period 1975–2000.

The effect of this rapid thinning could probably be reflected on the significant surface decrease and retreat that Gualas Glacier experienced between 2001 and 2011. During this period, Gualas Glacier lost 2.8 km^2 of its surface area which corresponds to 2.4 %

of the surface area of 2001 (Fig. 17). This percentage is equivalent to the percentage of surface area loss suffered by this glacier during the period 1979–2001. Therefore, the rate of shrinking more than doubled (from 0.1 $km^2 yr^{-1}$ to 0.28 $km^2 yr^{-1}$) between 2001 and 2011 compared to the period 1979–2001.

Gualas Glacier experiended a large retreat of 1.9 km between 2001 and 2011 corresponding to a rate of 190 $m yr^{-1}$ equivalent to 3 times larger than the rate of retreat estimated for 1979–2001.

According to Fig. 18, the tongue of Gualas Glacier must have disintegrated sometime between 2003 and 2005. This is supported by observations made through the orthoimage SPOT 5 of 18 May 2005 (Fig. 18, B) in which it is possible to observe that the frontal position of the glacier did not change significantly compared to 2011.

6.3 Reichert Glacier

Reichert Glacier is located on the north-western section of the NPI at 46°29′ S and 73°35′ W. It stretches between the highest point of 3700 m a.s.l. and the lowest point at 133 m a.s.l. Reichert Glacier has an ice area of 69.7 km^2 and a total length of 16.9 km (values obtained in this study based on the ETM+ Landsat satellite image of 19 February 2011).

As it possible to observe in Figs. 19 and 20, the geometry of Reichert Glacier exhibits a very narrow and elongated ablation area. This temperate glacier calves in a proglacial lake which is elongated as well in a NE-SW direction.

Reichert Glacier experienced one of the most significant retreats of the whole NPI and such recession produced important modifications on the morphology of the glacier. The recession of Reichert Glacier began before 1944–1945 as it is possible to observe on the glaciological map designed by Lliboutry (1956). Harrison and Winchester (1998) analyzed tree cores extracted from a trimline located on the western shore of Reichert lake. The oldest tree was dated 1876. Authors argued as well that large moraines marking the southern end of the Reichert proglacial lake were ice free by 1933 according to their dendrochronological dates.

Between 1945 and 1975 no changes were registered at the NE front and a small advance of 400 m was identified on the SW front (Aniya, 1992). Between 1975–1986 the NE snout retreated 2.3 km (214 m yr^{-1}). During the same period, the SW front retreated only 280 m (Aniya, 1992). The retreat of both fronts continued subsequently during the period 1986–1991 with 300–500 m and 850 m for the NE and SW fronts, respectively (Aniya, 1992). However, according to Aniya and Wakao (1997), between 1991 and 1994 the SW snout of Reichert Glacier disintegrated on the proglacial lake retreating 3.7 km (Aniya, 2007). After this period, very small recessions were registered for both snouts and during 1999 they merged into a single.

As shown in Fig. 20, Reichert Glacier experienced an important retreat (1.6 km) between 2001 and 2005 as seen in the ETM+ Landsat image of 11 March 2001 and the SPOT 5 satellite image of 18 May 2005. Between 2005 and 2011, no significant changes can be observed.

Rivera et al. (2007), estimated a thinning rate on 37 % of the ablation area of Reichert Glacier between 1975 and 2000 of 1.4 m yr^{-1} equivalent to 36.4 m in the period. This thinning is similar to that estimated by Rignot et al. (2003) (1.2 m yr^{-1}) for the period 1975–2000 covering the whole glacier.

Between 2001 and 2011, Reichert Glacier lost 1.7 km^2 which correspond to 2.4 % of the surface estimated for 2001. The shrinkage experienced by Reichert Glacier is very similar to that estimated for the period 1979–2001, meaning that Reichert Glacier has been shrinking very fast since at least 1979.

Reichert Glacier experienced such a reduction that the snout recessed into the fjord around 2002 (Aniya, 2007) as it is possible to observe in Fig. 20c. According to Lliboutry (1964) the geometry of the fjords plays an important role because it can accelerate the calving rate. When the glacier reaches a certain point in the retreating phase, it is no longer controlled by climate until it arrives in a narrower part of the fjord where it again becomes stable (Lliboutry, 1964).

The wasting of Reichert Glacier has been one of the most important of the NPI considering its surface area evolution and the frontal fluctuations of the glacier between 1979 and 2011.

7 Conclusions

In this paper, ice elevation changes of the NPI were analyzed by comparing three DEMs corresponding to 1975, 2000 and 2005. In addition, the glacier length fluctuations and the surface area evolution between 2001 and 2011 of 25 glaciers of the NPI were also studied. From a global point of view, the majority of the studied glaciers thinned, retreated and loss surface between 2001 and 2011, only few glaciers (Leones, Nef, Pared Sur and Soler) located on the eastern side of the NPI have been stable. Glaciers located on the western side of the NPI suffered a stronger wasting compared to the glaciers located on the eastern side.

We showed that overall, over the ablation areas of the NPI (below 1150 m a.s.l.) a more rapid thinning of 2.6 m yr^{-1} occurred between 2000 and 2005 yr compared to the period 1975–2000, in which a mean thinning of 1.7 m yr^{-1} was measured for the same zones of the NPI. For the whole period (1975–2005) the most important thinning of the ablation areas has been estimated for HPN-1 Glacier (4.4 m yr^{-1}) followed by Benito (3.4 m yr^{-1}), Fraenkel (2.4 m yr^{-1}), Gualas (2.1 m yr^{-1}) and Acodado (2.1 m yr^{-1}) glaciers, all of them located on the western side of the NPI. Above 1150 m a.s.l. the studied glaciers experienced a small thinning of 0.08 m between 2000 and 2005. If this thinning is maintained or increase with time it will generate a significant impact on the studied glaciers since it occurred over their accumulation areas.

Between 2001 and 2011, a noteworthy retreat was experienced by Gualas Glacier with 1.9 km, Reichert Glacier 1.6 km, both located on the north-western side of the NPI. On the south-western side of the NPI, Steffen Glacier experienced a remarkable retreat of 1.6 km between 2001 and 2011 as well. This glacier more than doubled its rate of retreat (compared to the 1979–2001 period) and experienced during this decennia the disintegration of its main front as well as a lateral tongue that retreated 3.1 km. The most significant retreat observed on the eastern side was experienced by Colonia Glacier (1 km).

Area loss was also relevant during the period 2001–2011. Overall, the icefield experienced a reduction of 50.6 km^2 which represents a 1.3 % relative to the surface area calculated for 2001 yr. The most remarkable surface reduction was observed for HPN-1 Glacier that loss 3.2 % of its surface estimated in 2001, followed by Steffen Glacier (2.8 %).

Variations of NPI's glaciers between 2001 and 2011 have been inducing important changes on the morphology of its surroundings. For instance, the accelerated retreat of Steffen Glacier triggered the enlargement of the surface area of its main proglacial lake (from 4.2 km^2 in 2001 to 9.4 km^2 in 2011), generating the increase of the river section of Rio Huemules.

We suggest that the glacier shrinking observed in the NPI is controlled firstly by atmospheric warming, as it has been reported in this area, however, updated climatic studies are needed in order to confirm this suggestion. If the detected past climate trends persist, in the future, glaciers of the NPI will continuous or even increase their rate of shrinking generating important consequences for this region like the production of GLOF events or the decrease of the melt-water runoff in the long-term future.

Acknowledgements. This study was sponsored by a FONDECYT postdoctoral grant (3095014) and by the Centre National d'Etudes Spatiales of France. The Spot 5 Digital Elevation Models and the SPOT 5 orthoimages used in this study were acquired in the framework of the Spot 5 Stereoscopic Survey of Polar Ice: Reference Images & Topographies (SPIRIT) project. ICESat data was obtained from the National Snow and Ice Data Center. The Landsat ETM+ satellite images used in this investigation were acquired through the USGS.

Special thanks are address to Jay Zwally for his valuable support for the ICESat data processing as well as to Etienne Berthier and Jérôme Korona for their initial exchanges related to this investigation.

Discussion Paper | Discussion Paper | Discussion Paper | Discussion Paper |

The publication of this article is financed by CNRS-INSU.

References

Aniya, M.: Glacier inventory for the Northern Patagonia Icefield, Chile, and variations 1944/45 to 1985/86, Arctic Alpine Res., 20, 179–187, 1988.

Aniya, M.: Glacier variation in the Northern Patagonia Icefield, Chile, between 1985/86 and 1990/91, Bulletin of Glaciological Research, 10, 83–90, 1992.

Aniya, M.: Recent glacier variations of the Hielos Patagonicos, South America, and their contribution to sea-level change, Arc. Antarct. Alp. Res., 31, 165–173, 1999.

Aniya, M.: Glacier variations of Hielo Patagonico Norte, Chilean Patagonia, since 1944/45, with special reference to variations between 1995/96 and 1999/2000, Bulletin of Glaciological Research, 18, 55–63, 2001.

Aniya, M.: Glacier variations of Hielo Patagonico Norte, Chile, for 1944/45–2004/05, Bulletin of Glaciological Research, 24, 59–70, 2007.

Aniya, M. and Enomoto, H.: Glacier variations and their causes in the Northern Patagonia Icefield, Chile, since 1944, Arctic Alpine Res., 18, 307–316, 1986.

Aniya, M. and Wakao, Y.: Glacier variations of Hielo Patagonico Norte, Chile, between 1944/45 and 1995/96, Bulletin of Glaciological Research, 15, 11–18, 1997.

Aniya, M., Casassa, G., and Naruse, R.: Morphology, surface characteristics, and flow velocity of Soler glacier, Patagonia, Arctic Alpine Res., 20, 414–421, 1988.

Aniya, M., Sato, H., Naruse, R., Skvarca, P., and Casassa, G.: Recent glacier variations in the Southern Patagonia Icefield, South America, Arctic Alpine Res., 29, 1–12, 1997.

Aniya, M., Dhakal, A., Park, S., and Naruse, R.: Variations of patagonian glaciers, South America, using RADARSAT and Landsat images, Can. J. Remote Sens., 26, 501–511, 2000.

Aniya, M., Skvarca, P., Sugiyama, S., Aoki, T., Matsumoto, T., Anma, R., Naito, N., Enomoto, H., Hori, K., Marinsek, S., Konya, K., Nuimura, T., Tsutaki, S., Tone, K. and Barcaza, G.: Glaciological research project in Patagonia 2006-2009: studies at Perito Moreno, Hielo Patagónico Norte, and along the Pacific coast, Bulletin of Glaciological Research, 29, 1–17, 2011.

Bamber, J. and Payne, A. (Eds.): Mass balance of the Cryosphere. Observations and modelling of contemporary and future changes, Cambridge University Press, Cambridge, 644 pp., 2004.

Barcaza, G., Aniya, M., Matsumoto, T., and Aoki, T.: Satellite-Derived Equilibrium Lines in Northern Patagonia Icefield, Chile, and Their Implications to Glacier Variations, Arct. Antarc. Alp. Res., 41, 174–182, 2009.

Berthier, E. and Toutin, T.: SPOT5-HRS digital elevation models and the monitoring of glacier elevation changes in North-West Canada and South-East Alaska, Remote Sens. Environ., 112, 2443–2454, 2008.

Berthier, E., Arnaud, Y., Vincent, C., and Rémy, F.: Biases of SRTM in high-mountain areas. Implications for the monitoring of glacier volume changes, Geophys. Res. Lett., 33, L08502, doi:10.1029/2006GL025862, 2006.

Berthier, E., Arnaud, Y., Kumar, R., Ahmad, S., Wagnon, P., and Chevallier, P.: Remote sensing estimates of glacier mass balances in the Himachal Pradesh (Western Himalaya, India), Remote Sens. Environ., 108, 327–338, 2007.

Carrasco, J., Casassa, G., and Rivera, A.: Meteorological and climatological aspects of the Southern Patagonia Icefield, in: The Patagonian Icefields. A unique Natural Laboratory for Environmental and Climate Change Studies, edited by: Casassa, G., Sepulveda, F., and Sinclair, R., Kluwer Academic/Plenum Publishers, New York, 29–65, 2002.

Casassa, G.: Glacier inventory in Chile: current status and recent glacier variations, Ann. Glaciol., 21, 317–322, 1995.

Casassa, G. and Marangunic, C.: Exploration history of the Northern Patagonia Icefield, Bulletin of Glaciological Research, 4, 163–175, 1987.

Casassa, G., Brecher, H., Rivera, A., and Aniya, M.: A century-long recession record of Glaciar O'Higgins, Chilean Patagonia, Ann. Glaciol., 24, 106–110, 1997.

Casassa, G., Sepulveda, F., and Sinclair, R. (Eds.): The Patagonian Icefields, Kluwer Academic/Plenum Publishers, Valdivia, Chile, 192 pp., 2002.

Casassa, G., López, P., Pouyaud, B., and Escobar, F.: Detection of changes in glacial runoff in alpine basins: examples from North America, central Asia and the Andes (invited paper),

Hydrol. Process., 23, 31–41, 2009.
Casassa, G., Wendt, J., Wendt, A., López, P., Schuler, T., Maas, H., Carrasco, J., and Rivera, A.: Outburst floods of glacial lakes in Patagonia: is there an increasing trend?, EGU General Assembly 2010, Vienna, Austria, 2–7 May 2010, 2010.
Farr, T., Rosen, P., Caro, E., Crippen, R., Duren, R., Hensley, S., Kobrick, M., Paller, M., Rodriguez, E., Roth, L., Seal, D., Shaffer, S., Shimada, J., Umland, J., Werner, M., Oskin, M., Burbank, D., and Alsdorf, D.: The Shuttle Radar Topographic Mission, Rev. Geophys., 45, RG2004, doi:10.1029/2005RG000183, 2007.
Glasser, N., Harrison, S., Jansson, K., Anderson, K., and Cowley, A.: Global sea-level contribution from the Patagonian Icefields since the Little Ice Age maximum, Nat. Geosci., 4, 303–307, 2011.
Harrison, S. and Winchester, V.: Historical fluctuations of the Gualas and Reicher Glaciers, North Patagonian Icefield, Chile, The Holocene, 8, 481–485, 1998.
Hock, R.: Glacier melt: a review of processes and their modelling, Prog. Phys. Geogr., 29, 362–391, 2005.
Ibarzabal, T., Hoffmann, J., and Naruse, R.: Recent climate changes in southern Patagonia, Bulletin of Glaciological Research, 14, 29–36, 1996.
IPCC: Climate Change 2007: The Physical Science Basis. Summary for Policymakers, in: Contribution of Working Group I to the Fourth Assessment Report of the Intergovernmental Panel on Climate Change, Geneva, 2007.
Kääb, A.: Remote sensing of mountain glaciers and permafrost creep. Glaziologie und Geomorphodynamik, Geographisches Institut der Universität Zürich, Zürich, 264 pp., 2005.
Korona, J., Berthier, E., Bernard, M., Rémy, F., and Thouvenot, E.: SPOT 5 stereoscopic survey of Polar Ice: Reference Images and Topographies during the fourth International Polar Year (2007–2009), ISPRS J. Photogramm., 64, 204–212, doi:10.1016/j.isprsjprs.2008.10.005, 2009.
Lliboutry, L.: Nieves y glaciares de Chile, Fundamentos de glaciologia, Santiago, 471 pp., 1956.
Lliboutry, L.: Traité de glaciologie, 2. Masson, Paris, 1040 pp., 1964.
López, P., Casassa, G., and Delclaux, F.: Future of the water resources of a high glacierized basin located in Patagonia, Chile, HydroPredict'2010. International Interdisciplinary Conference on Predictions for Hydrology, Ecology and Water Resources Management. Changes and Hazards caused by Direct Human Interventions and Climate Change, Prague, Czech

TCD
5, 3323–3381, 2011

Republic, 2010a.
López, P., Chevallier, P., Favier, V., Pouyaud, B., Ordenes, F., and Oerlemans, J.: A regional view of fluctuations in glacier length in southern South America, Global Planet. Change, 71, 85–108, 2010b.
López , P., Casassa, G., Ulloa, D., and Espinoza, F.: Water in Patagonian glaciers and climate change, The case of Nef river catchment basin, in prep., 2011.
Nuth, C. and Kääb, A.: Co-registration and bias corrections of satellite elevation data sets for quantifying glacier thickness change, The Cryosphere, 5, 271–290, doi:10.5194/tc-5-271-2011, 2011.
Oerlemans, J.: Glaciers and Climate Change, A. A. Balkema, Rotterdam, 148 pp., 2001.
Ohata, T., Kondo, H., and Enomoto, H.: Meteorological observations at San Rafael Glacier, in: Glaciological studies in Patagonia Northern Icefield 1983–1984, edited by: Nakajima, C., Data Center for Glacier Research, Japanese Society of Snow and Ice, Nagoya, 22–31, 1985.
Paul, F.: Calculation of glacier elevation changes with SRTM: is there an elevation-dependent bias?, J. Glaciol., 54, 945–946, 2008.
Rasmussen, L., Conway, H., and Raymond, C.: Influence of upper air conditions on the Patagonia Icefields, Global Planet. Change, 59, 203–216, 2007.
Rignot, E., Echelmeyer, K., and Krabill, W.: Penetration depth of interferometric synthetic-aperture radar signals in snow and ice, Geophys. Res. Lett., 28, 3501, 3501–3504, 2001.
Rignot, E., Rivera, A., and Casassa, G.: Contribution of the Patagonia Icefields of South America to Sea Level Rise, Science, 302, 434–437, 2003.
Rivera, A., Benham, T., Casassa, G., Bamber, J., and Dowdeswell, J.: Ice elevation and areal changes of glaciers from the Northern Patagonia icefield, Chile, Global Planet. Change, 59, 126–137, 2007.
Rosenblüth, B., Casassa, G., and Fuenzalida, H.: Recent climatic changes in western Patagonia, Bulletin of Glaciological Research, 13, 127–132, 1995.
Skvarca, P. and De Angelis, H.: First cloud-free Landsat TM image mosaic of Hielo Patagonico Sur, South Western Patagonia, South America, Intituto Antartico Argentino, Buenos Aires, 2002.
Warren, C., Glasser, N., Harrison, S., Winchester, V., Kerr, A., and Rivera, A.: Characteristics of tide-water calving at Glaciar San Rafael, Chile, J. Glaciol., 41, 273–289, 1995.
Zwally, J., Schutz, B., Abdalati, W., Abshire, J., Bentley, C., Brenner, A., Bufton, J., Dezio, J.,

TCD
5, 3323–3381, 2011

Recent acceleration of ice loss in the Northern Patagonia Icefield

P. López and G. Casassa

Hancock, D., Harding, D., Herring, T., Minster, B., Quinn, K., Palm, S., Spinhirne, J., and Thomas, R.: ICESat's laser measurements of polar ice, atmosphere, ocean, and land, J. Geodyn., 34, 405–445, 2002.

Table 1. Surface of the NPI covered by every DEM used in this investigation.

DEM	Surface NPI (km^2)	Surface over 1150 m a.s.l. (km^2)	%	Surface below 11 150 m a.s.l. (km^2)	%
1975 Topo	1930	1062.9	55	867.4	50
2000 SRTM	3794	2326.7	61	1467.4	38.6
2005 SPIRIT	2946	1718	58.3	1228.5	41.6

TCD
5, 3323–3381, 2011

TCD
5, 3323–3381, 2011

Table 2. Surface of the NPI covered by every pair-wise of DEMs considered in this investigation.

Pair-wise	Surface NPI (km^2)	% of the total NPI's surface	Surface over 1150 m a.s.l. (km^2)	%	Surface below 11 150 m a.s.l. (km^2)	%
1975–2000	1850	46.7	961.6	40	867.4	56
2000–2005	2910	73.6	1681.6	70.2	1228.4	78.8
1975–2005	1494	37.8	776.5	32.4	717.2	46

Table 3. Description of the Landsat satellite images used in this study.

Sensor	Acquisition date	Bands used in this study	Bandwidth (µm)	Spatial resolution	Source
MSS	22 January 1979	4 5 6	0.52–0.60 0.63–0.69 0.76–0.90	60 m	USGS
ETM+	11 March 2001 & 19 February 2011	1 4 5	0.45–0.51 0.76–0.90 1.55–1.75	30 m	

TCD
5, 3323–3381, 2011

Recent acceleration of ice loss in the Northern Patagonia Icefield

P. López and G. Casassa

Table 4. Horizontal shift estimated for the comparison of every DEM with IceSat data.

DEM	Dh Initial (m)	Dh Final (m)	σ Initial	σ Final	Records	a (m)	b (radians)	DX	DY
1975–IS	9.5	6.7	36.1	24.6	1959	0.8	1.9	−48.1	26.7
2000–IS	−1.5	−0.6	34.9	14.5	2264	2	0.4	71.2	8.1
2005–IS	−6.3	−6.3	19.5	17.9	1717	0.28	1.0	−1.3	−14.6

TCD
5, 3323–3381, 2011

Table 5. Comparison of DEMs over the non glacierized area.

Period	Dh	σ	Records
1975–2005	−0.95	27.5	93283
2000–2005	0.2	24.2	93696
1975–2000	−1.36	24.8	94020

TCD
5, 3323–3381, 2011

Table 6. Mean thinning rates for the NPI.

Period	Thinning rate ($m\,yr^{-1}$)	Records
1975–2000	−0.73	407746
1975–2005	−0.81	348544
2000–2005	−1.12	800985

TCD
5, 3323–3381, 2011

P. López and G. Casassa

Table 7. Mean thinning rates of the NPI below 1150 m a.s.l.

Period	Thinning rate ($m\,yr^{-1}$)	Records
1975–2000	−1.7	239130
1975–2005	−2.36	198063
2000–2005	−2.64	340817

TCD
5, 3323–3381, 2011

P. López and G. Casassa

Table 8. Comparison of ice elevation changes obtained in previous studies with the results estimated in this investigation.

Glacier	Dh 1975–2000 (this paper) (*)	Dh 1975–2001 (Rivera et al. 2007) (*)	Dh 1975–2000 (Rignot et al. 2003)	Dh 2000–2005 (this paper) (*)	Dh 1975–2005 (this paper) (*)
Acodado	−2.1	−2.1		−1.6	−2.1
Bayo	−1.2	−1.3		−2.6	−1.4
Benito	−3.1	−3.0	−1.4	−2.4	−3.4
Cachet	−2.2	−2.2		−2.5	−2.2
Colonia	−1.0	−1.1	−0.5	−2.3	−1.5
Fraenkel	−2.4	−2.4	−0.9	−2.6	−2.4
Grosse	−1.2	−1.1	−1.6	−2.6	−1.7
Gualas	−2.0	−2.0	−1.3	−2.7	−2.1
HPN-1	−4.2	−4.0	−2.2	−4.2	−4.4
Nef	−1.1	−1.9	−0.6	−2.3	−1.3
Pared Norte			−1.1		−1.6
Pared Sur	−1.1	−1.0	−1.2	−1.3	−1.2
Reichert	−1.8	−1.4	−1.2		
San Quintin	−1.6	−1.7	−0.6	−1.9	−1.6
Soler	−2.2	−2.5	−0.6	−2.9	−2.2
Steffen	−1.7	−1.5	−1.1		
Strindberg	−1.8	−1.6	−0.9	−1.5	−1.7

(*) Below the ELA estimated by Rivera et al. (2007) for every glacier

Discussion Paper | Discussion Paper | Discussion Paper | Discussion Paper |

TCD

5, 3323–3381, 2011

Recent acceleration of ice loss in the Northern Patagonia Icefield

P. López and G. Casassa

Table 9. Length changes of 1979–2001 and 2001–2011 of the studied glaciers.

Glacier	Latitude	Longitude	Length 2011 (km)	Length changes (km) 1979–2001	Length changes (km) 2001–2011
Acodado	−47.3	−73.8	42.3	−1.1	−0.9
Arco	−47.2	−73.2	11.1	−1.5	0
Benito	−47.1	−73.7	30.9	−0.6	−0.0
Cachet	−47.1	−73.4	13.1	−1.2	−0.2
Colonia	−47.2	−73.4	37.4	−0.5	−0.9
Fiero	−46.7	73.2	13.7	−0.6	−0.4
Fraenkel	−46.9	−73.6	13.0		−0.5
Gualas	−46.6	−73.5	27.4	−1.2	−1.9
HPN-1	−47.2	−73.7	23.7	−0.1	−0.9
HPN-4	−47.4	−73.5	17.0	−0.5	−0.2
Leones	−46.8	−73.3	12.3	−0.4	−0.0
Nef	−47.0	−73.3	29.3	−3.3	−0.0
Pared Norte	−47.4	−73.4	23.9	−0.5	−0.4
Pared Sur	−47.4	−73.3	12.6	−1.2	−0.1
Pissis	−47.5	−73.4	8.0	−0.3	−0.4
Reichert	−46.4	−73.5	16.8	−4.9	−1.6
San Quintín	−46.9	−73.6	65.9	−1.8	0.0
San Rafael	−46.7	−73.5	51.6	−4.0	−0.09
Soler	−46.9	−73.3	17.1	−0.4	0
Steffen	−47.3	−73.6	46.6	−1.5	−1.6
Strindberg	−46.9	−73.7	5.5		−0.6
U-2	−47.4	−73.5	7.0	−0.5	−0.04
U-3	−47.4	−73.4	9.9	−0.8	0
U-4	−47.3	−73.3	5.5	−1.4	−1.2
U-5	−47.0	−73.3	5.7	−0.4	0

TCD
5, 3323–3381, 2011

Table 10. Surface changes of 1979–2001 and 2001–2011 of the studied glaciers.

Glacier	Latitude	Longitude	Ice area 2011 (km^2)	Ice area change 1979–2001 (%)	Ice area change 2001–2011 (%)
Acodado	−47.3	−73.8	263.7	−4.4	−1.7
Arco	−47.2	−73.2	25.9	−1.9	−0.02
Benito	−47.1	−73.7	158.5	−4.0	−1.7
Cachet	−47.1	−73.4	36.9	−6.0	−0.5
Colonia	−47.2	−73.4	284.6	−3.1	−1.1
Fiero	−46.7	73.2	41.1	−3.1	−0.8
Fraenkel	−46.9	−73.6	30.2	−5.4	−2.4
Gualas	−46.6	−73.5	116.3	−2.4	−2.3
HPN-1	−47.2	−73.7	148.2	−5.7	−3.2
HPN-4	−47.4	−73.5	64.9	−2.4	−0.5
Leones	−46.8	−73.3	66.4	−0.7	0.0
Nef	−47.0	−73.3	126.9	−5.8	0.0
Pared Norte	−47.4	−73.4	79.5	−0.8	−0.9
Pared Sur	−47.4	−73.3	31.8	−5.5	0.0
Pissis	−47.5	−73.4	12.3	−9.2	−1.9
Reichert	−46.4	−73.5	69.7	−6.2	−2.4
San Quintín	−46.9	−73.6	776.7	−4.0	−1.6
San Rafael	−46.7	−73.5	718.5	−1.9	−0.4
Soler	−46.9	−73.3	50.2	−4.8	0.0
Steffen	−47.3	−73.6	416.3	−2.6	−2.7
Strindberg	−46.9	−73.7	16.5	−6.8	−2.0
U-2	−47.4	−73.5	15.9	−2.6	−0.01
U-3	−47.4	−73.4	17.8	−3.5	−0.09
U-4	−47.3	−73.3	12.6	−3.4	−3.5
U-5	−47.0	−73.3	4.9	−19.6	−0.02

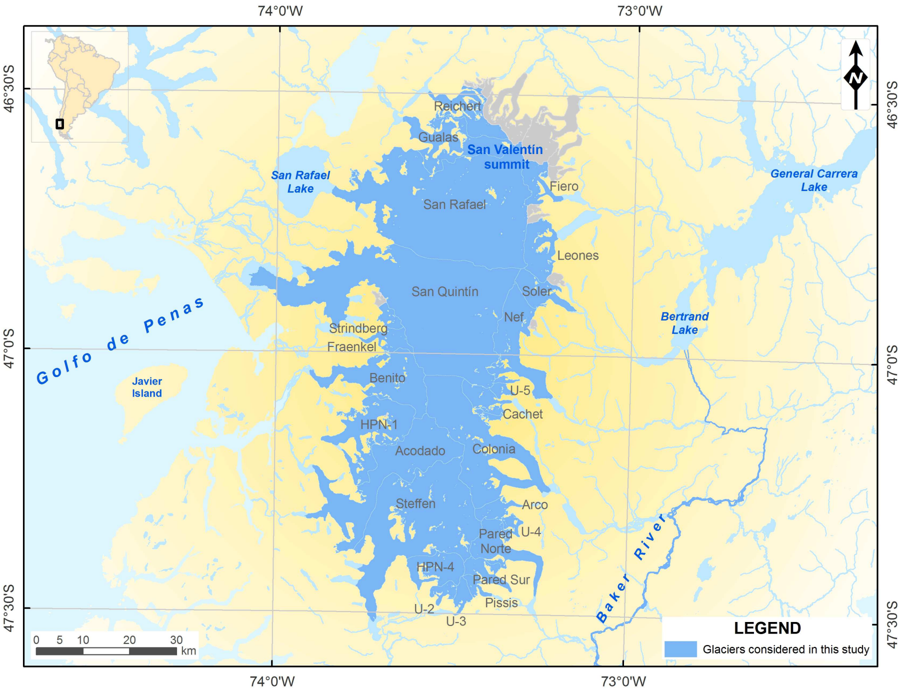

Fig. 1. The Northern Patagonia Icefield and the glaciers studied in this investigation.

TCD
5, 3323–3381, 2011

Recent acceleration of ice loss in the Northern Patagonia Icefield

P. López and G. Casassa

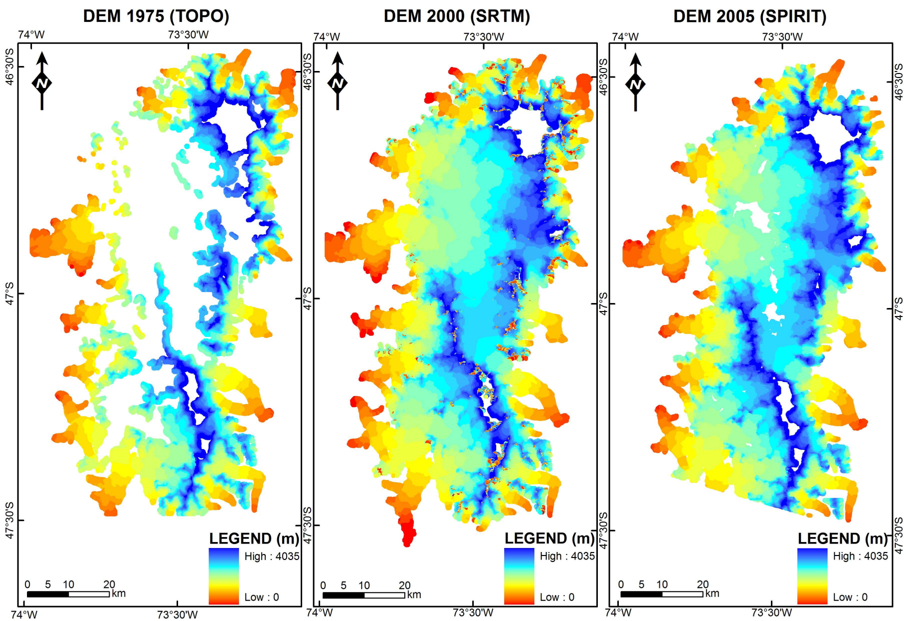

Fig. 2. The DEMs used in this investigation.

TCD
5, 3323–3381, 2011

Recent acceleration of ice loss in the Northern Patagonia Icefield

P. López and G. Casassa

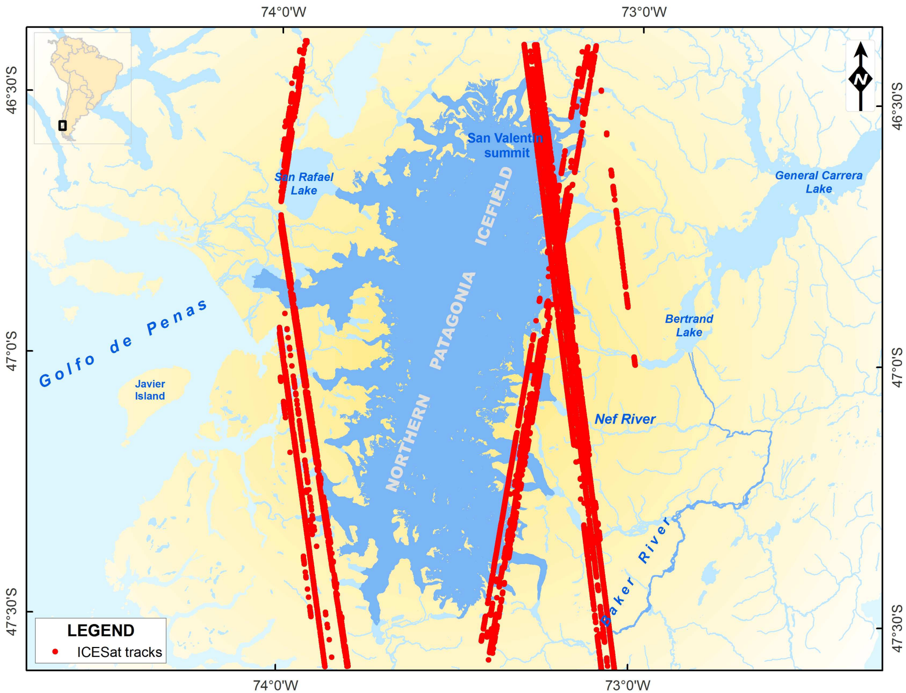

Fig. 3. ICESat tracks over the NPI.

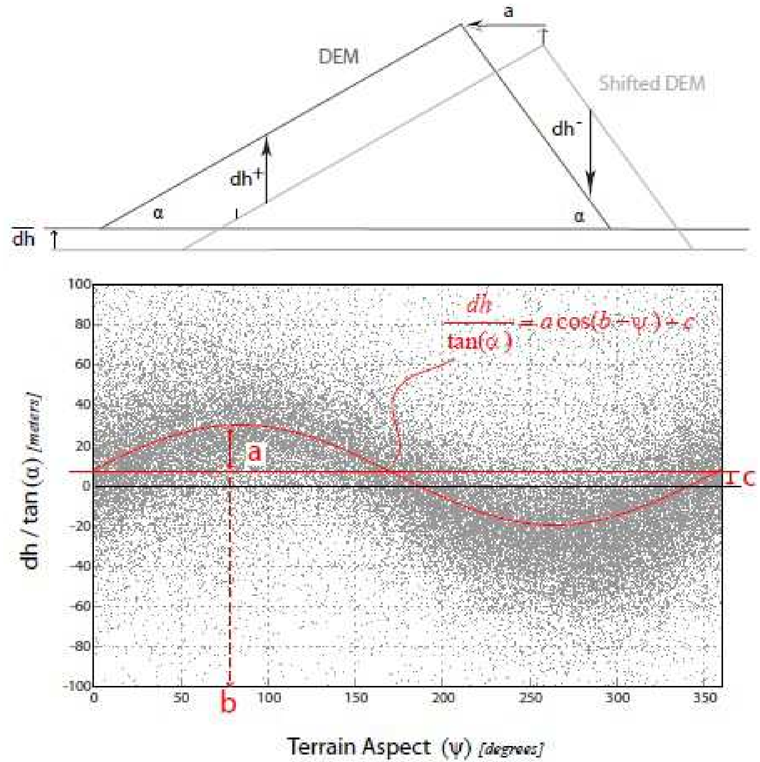

Fig. 4. Published by Nuth and Kääb (2011): Top: 2-D scheme of elevation differences induced by a DEM shift. Bottom: The scatter of elevation differences between 2 DEMs showing the relationship between the vertical deviations normalized by the slope tangent (y-axis) and terrain aspect (x-axis).

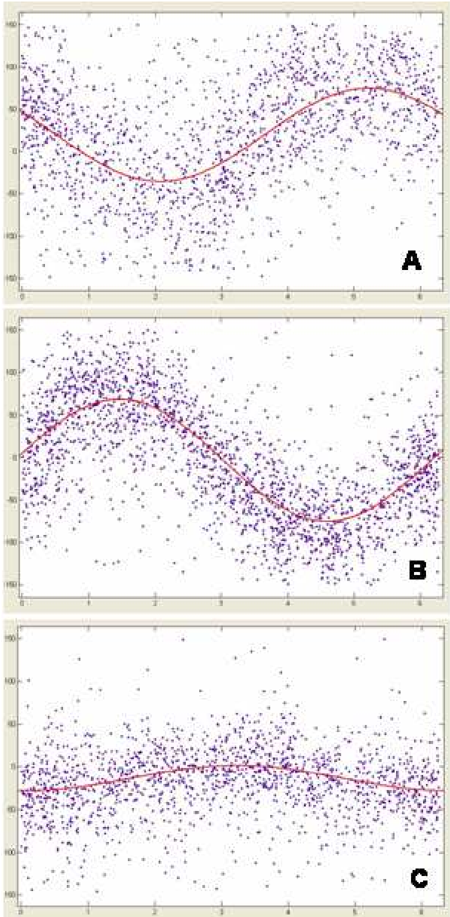

Fig. 5. Scatter plot of the dh/tan(α) (Y axis) and the terrain aspect (X axis) for the DEM 1975 (A), the SRTM (B) and the SPOT 5 DEM of 2005 (C).

TCD

5, 3323–3381, 2011

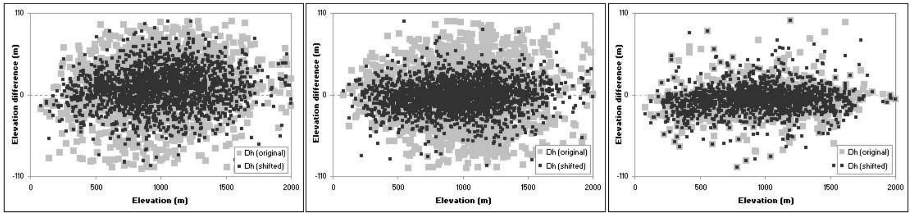

Fig. 6. Comparison of the original and shifted data for (from the left to the right) the 1975 DEM, SRTM and SPOT 5 DEM of 2005.

TCD
5, 3323–3381, 2011

Recent acceleration of ice loss in the Northern Patagonia Icefield

P. López and G. Casassa

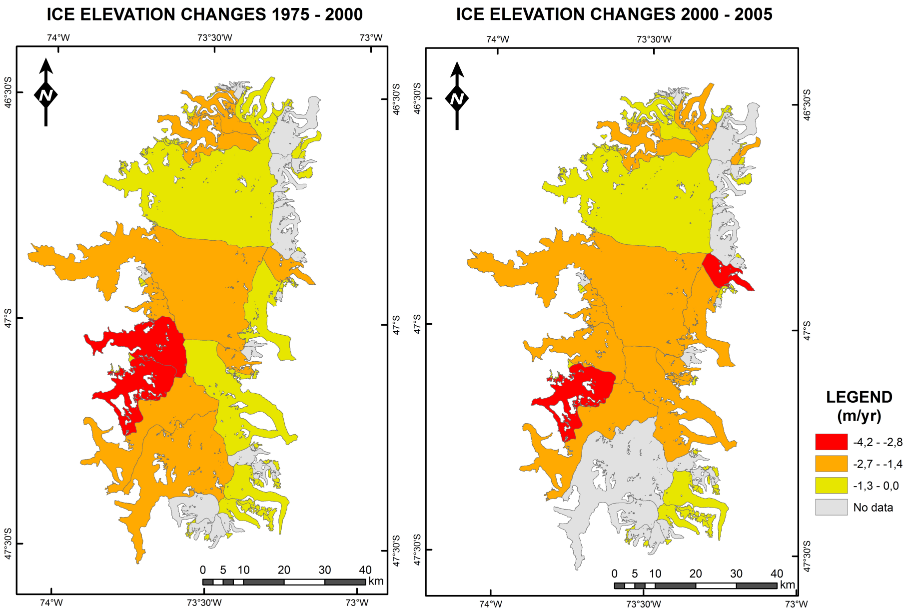

Fig. 7. Ice elevation changes per glacier for 1975–2000, 1975–2005 and 2000–2005 periods.

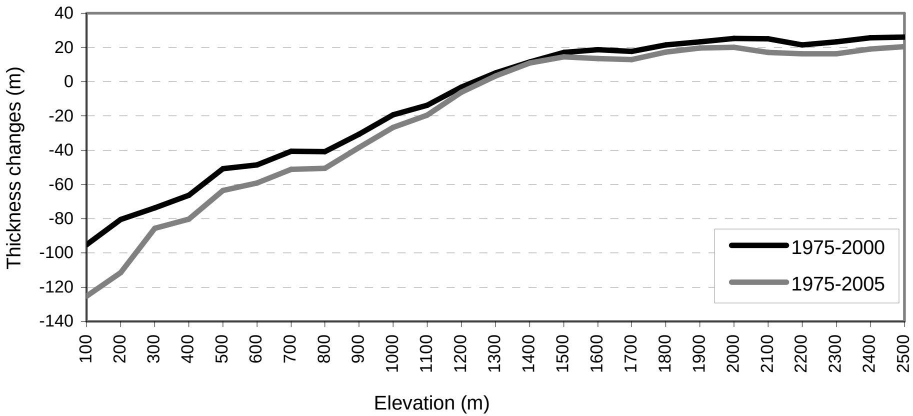

Fig. 8. Ice elevation changes of the NPI between 1975 and 2005 according to the elevation.

TCD
5, 3323–3381, 2011

Recent acceleration of ice loss in the Northern Patagonia Icefield

P. López and G. Casassa

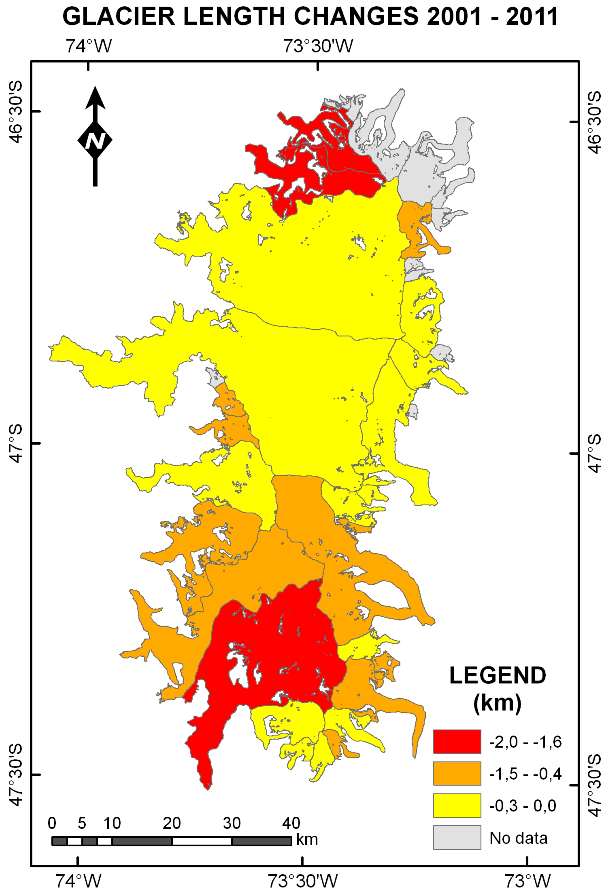

Fig. 9. Glacier length fluctuations of the NPI between 2001 and 2011.

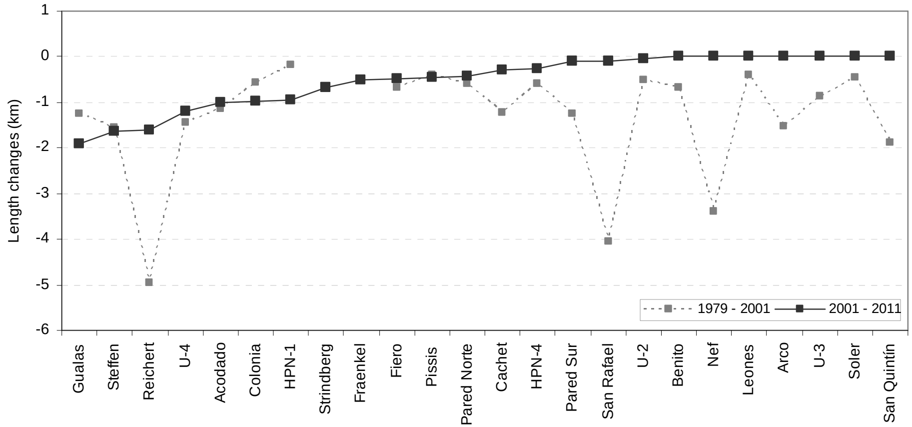

Fig. 10. Glacier length fluctuations of the NPI for 1979–2001 and 2001–2011 periods.

TCD
5, 3323–3381, 2011

Recent acceleration of ice loss in the Northern Patagonia Icefield

P. López and G. Casassa

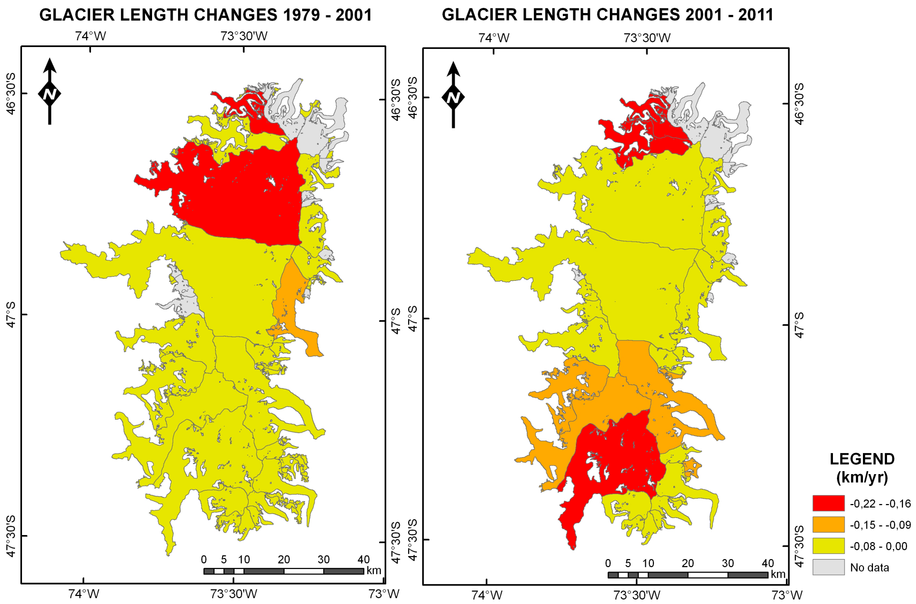

Fig. 11. Glacier length fluctuations of the NPI for 1979–2001 and 2001–2011.

TCD
5, 3323–3381, 2011

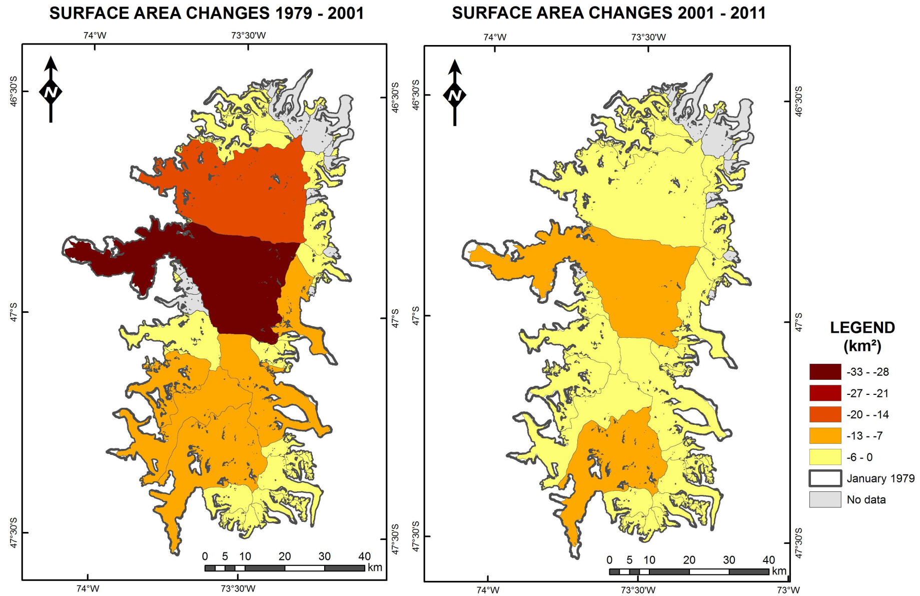

Fig. 12. Surface area variations of the NPI for 1979–2001 and 2001–2011 periods.

TCD
5, 3323–3381, 2011

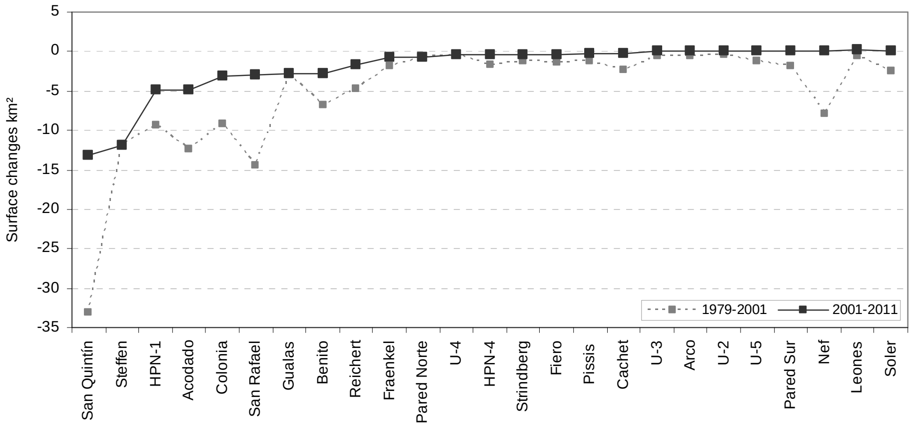

Fig. 13. Surface area variations of the NPI for 1979–2001 and 2001–2011 periods.

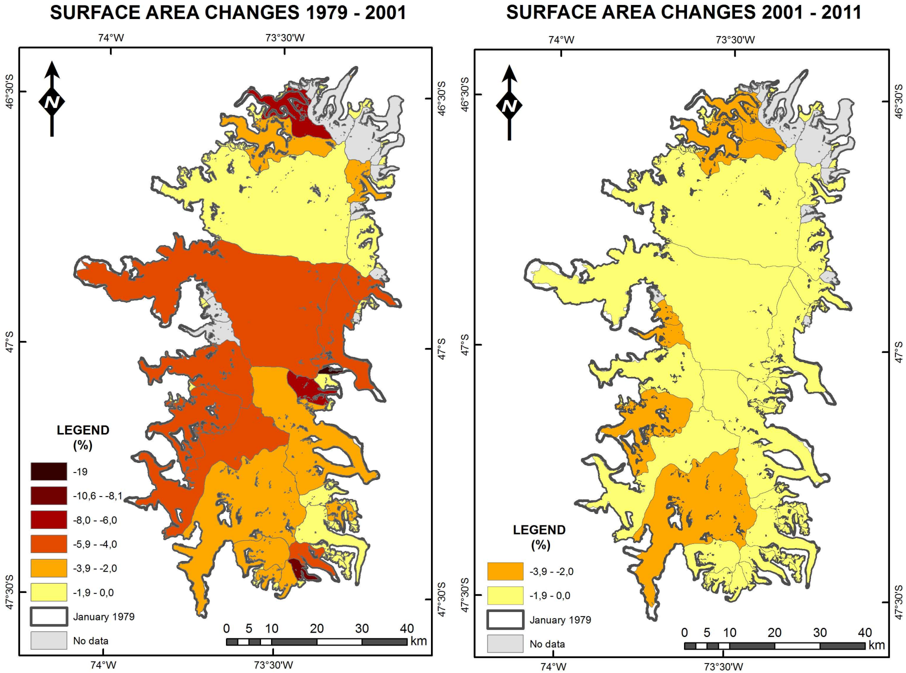

Fig. 14. Surface area variations (%) of the NPI for 1979–2001 and 2001–2011.

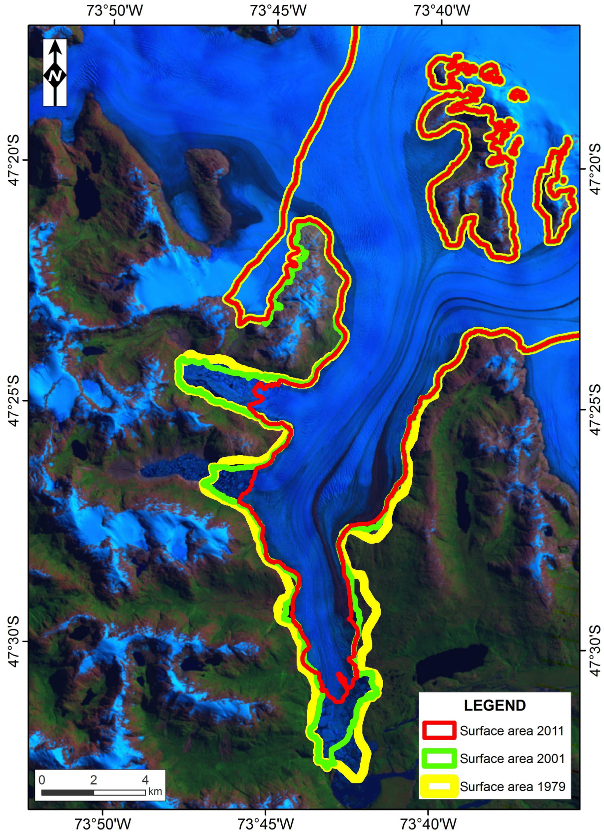

Fig. 15. Fluctuations of Steffen Glacier between 1979 and 2011 represented over the false-color composite of the Landsat ETM+ satellite image of 19 February 2011.

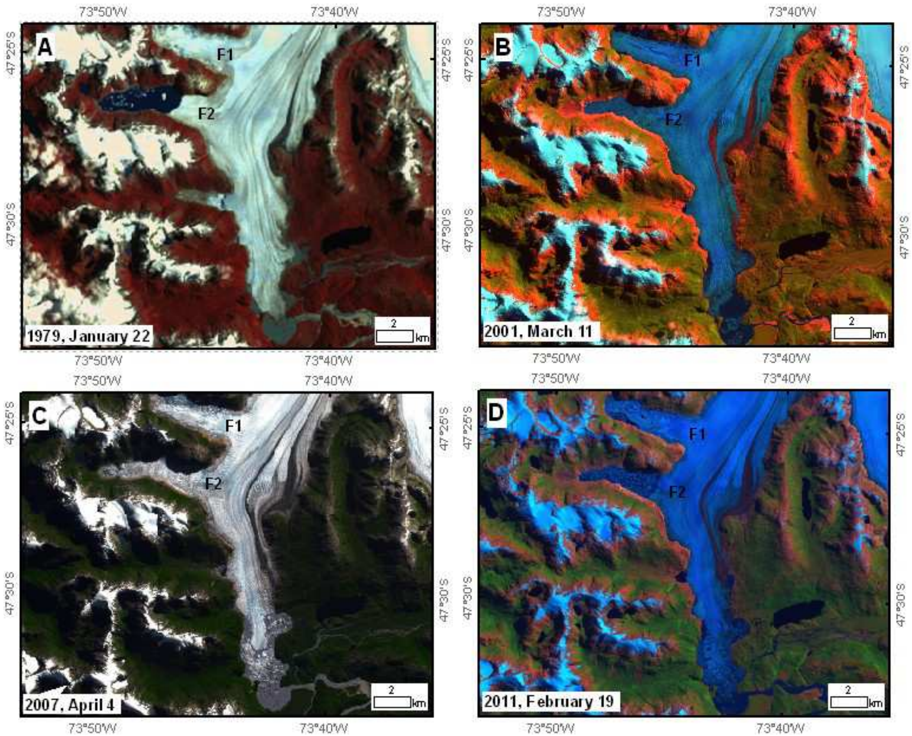

Fig. 16. Frontal position of Steffen Glacier. **(A)** False-color composite of the Landsat MSS satellite image of 22 January 1979. **(B)** False-color composite of the Landsat ETM+ satellite image of 11 March 2001. **(C)** ASTER Terra look image of 4 April 2007. **(D)** False-color composite of the Landsat ETM+ satellite image of 19 February 2011. Every image is represented in UTM projection 18 South zones and datum WGS 84.

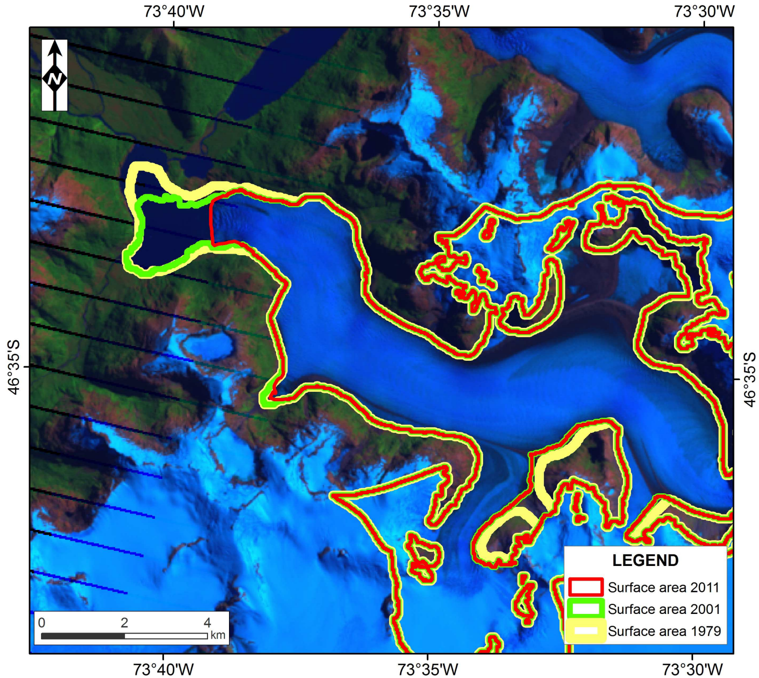

Fig. 17. Fluctuations of Gualas Glacier between 1979 and 2011 represented over the false-color composite of the Landsat ETM+ satellite image of 19 February 2011.

TCD
5, 3323–3381, 2011

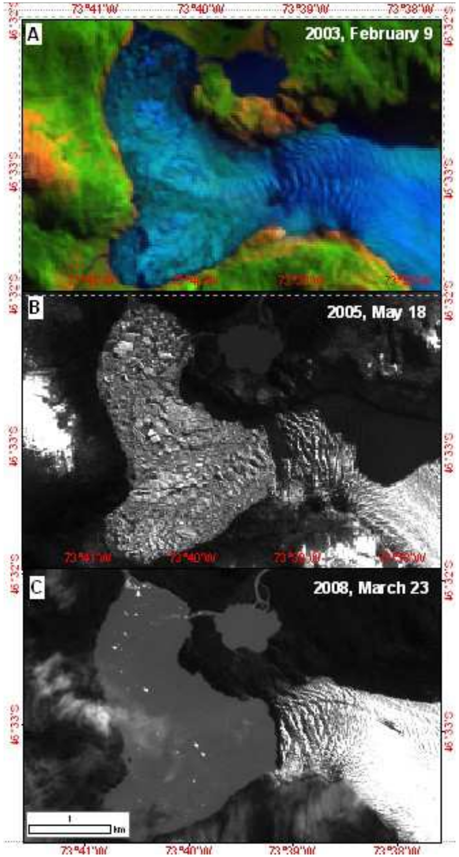

Fig. 18. Frontal position of Gualas Glacier. **(A)** False-color composite of the Landsat ETM+ satellite image of 9 February 2003. **(B)** Ortho-image SPOT 5 of 18 May 2005. **(C)** Ortho-image SPOT 5 of 23 March 2008. Every image is represented in UTM projection 18 South zones and datum WGS 84.

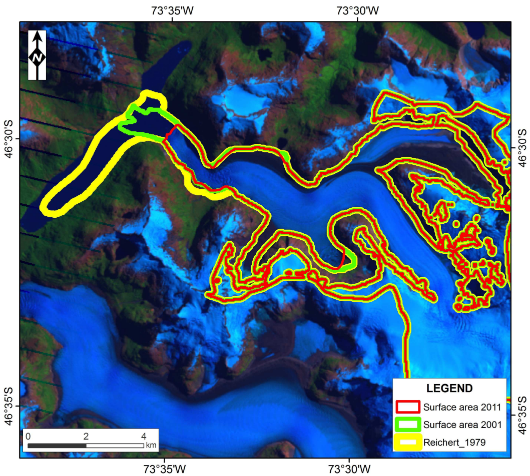

Fig. 19. Fluctuations of Reichert Glacier between 1979 and 2011 represented over the false-color composite of the Landsat ETM+ satellite image of 19 February 2011.

TCD
5, 3323–3381, 2011

Title Page
Abstract | Introduction
Conclusions | References
Tables | Figures
◀| |▶
◀ ▶
Back | Close
Full Screen / Esc
Printer-friendly Version
Interactive Discussion

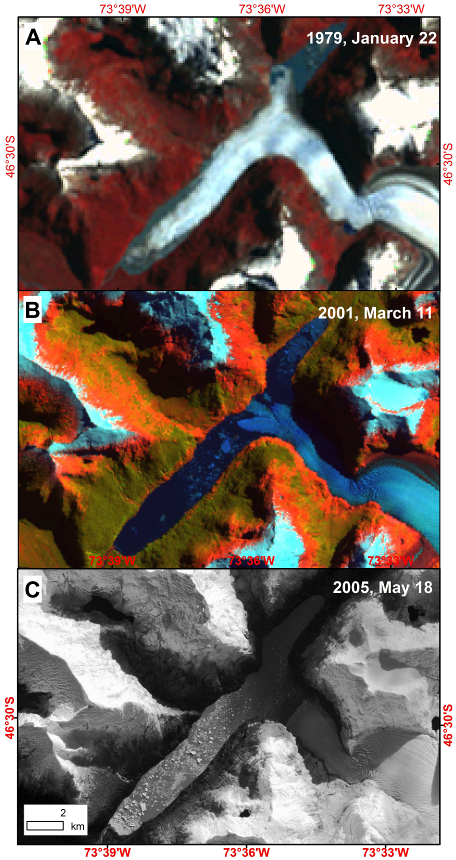

Fig. 20. Frontal position of Reichert Glacier. **(A)** False-color composite of the Landsat MSS satellite image of 22 January 1979. **(B)** False-color composite of the Landsat ETM+ satellite image of 11 March 2001. **(C)** Ortho-image SPOT 5 of 18 May 2005. Every image is represented in UTM projection 18 South zone and datum WGS 84.